Current carriers near dipolarization fronts in the magnetotail: A THEMIS event study

X.-J. Zhang,[1] V. Angelopoulos,[1] A. Runov,[1] X.-Z. Zhou,[1] J. Bonnell,[2] J. P. McFadden,[2] D. Larson,[2] and U. Auster[3]

Received 1 July 2010; revised 16 November 2010; accepted 30 November 2010; published 25 January 2011.

[1] We study current carriers observed within thin current sheets ahead of and during the passage of earthward moving dipolarization fronts in the near-Earth plasma sheet using Time History of Events and Macroscale Interactions During Substorms (THEMIS) multipoint measurements. The fronts are embedded within flow bursts at the initial stage of bursty bulk flow events. Simultaneous north-south and radial separations between probes P3, P4, and P5 and the planar current sheet approximation enable estimation of cross-tail current density in the current sheet ahead of and within the fronts, respectively. The cross-tail current density increase ahead of the fronts, a substorm growth phase signature, is predominantly due to the ion diamagnetic current; at times, however, the electron pressure gradient may contribute up to 60% of the total current density. Note that in this paper we refer to the horizontal (vertical) current sheet as the cross-tail current sheet (current sheet associated with dipolarization fronts). At the dipolarization fronts, the horizontal cross-tail current sheet (with a current density of several nA/m^2) relaxes, and a vertical current sheet (with a current density of several tens of nA/m^2), consistent with the thin interface of the front, appears. Thus, the cross-tail current at longitudes adjacent to the flow burst feeds into the dipolarization front's current sheet and may be extended to higher latitudes. The vertical current density also decreases after passage of the front. The pressure gradient of 1–10 keV electrons is a dominant contributor to the current in the dipolarization fronts. In the event studied, probes P1 and P2, which were several Earth radii downtail, reveal a tailward expansion of the current reduction process at a propagation velocity ~50 km/s, even as the bulk flow carrying the magnetic flux remains earthward. This study shows how dipolarization fronts and their current systems are building blocks of the large-scale substorm current wedge.

Citation: Zhang, X.-J., V. Angelopoulos, A. Runov, X.-Z. Zhou, J. Bonnell, J. P. McFadden, D. Larson, and U. Auster (2011), Current carriers near dipolarization fronts in the magnetotail: A THEMIS event study, *J. Geophys. Res.*, *116*, A00I20, doi:10.1029/2010JA015885.

1. Introduction

[2] Thin current sheets in the magnetotail are a key element of magnetospheric substorms [*Pulkkinen et al.*, 1994; *Baumjohann et al.*, 2007]. In the past it has been difficult, however, to examine magnetotail current sheet structure and its evolution as inferred from particle observations on single spacecraft because noise (e.g., thermal noise of electron distributions or temporal aliasing) and offset sources (e.g., asymmetry of spacecraft potential) typically dominate the signal. Multipoint observations for study of current sheet structure and dynamics, are essential for determining an absolute integrated current density between the spacecraft that can then be compared with plasma measurements of local current densities. Significant progress in current sheet studies was made using two-point ISEE 1 and 2 [*Pulkkinen et al.*, 1994; *Sanny et al.*, 1994] and four-point Cluster [*Runov et al.*, 2003, 2006; *Thompson et al.*, 2005; *Petrukovich et al.*, 2007] observations. Since then, the five-probe Time History of Events and Macroscale Interactions During Substorms (THEMIS) mission [*Angelopoulos*, 2008] has contributed equatorial multipoint measurements that can be used in such studies. In the 2009 tail science season (mid-December-April [see *Sibeck and Angelopoulos*, 2008]), three THEMIS probes monitored magnetotail current sheet dynamics at a geocentric distance of 11 Earth radii (R_E), i.e., in the transition region between tail-like and dipole-dominated plasma sheet, from both horizontal (X_{GSM}, Y_{GSM}) and vertical (Z_{GSM}) separations. This region plays a key role in magnetospheric dynamics during substorms, and recent THEMIS studies have

[1]Institute of Geophysics and Planetary Physics, University of California, Los Angeles, California, USA.
[2]Space Sciences Laboratory, University of California, Berkeley, California, USA.
[3]Institut für Geophysik und Extraterrestrische Physik, Technische Universität Braunschweig, Braunschweig, Germany.

0148-0227/11/2010JA015885

revealed that the evolution of substorm phenomena on the ground can be correlated with the evolution of the substorm current wedge in space at that location [e.g., *Angelopoulos et al.*, 2008].

[3] Thinning and stretching of the plasma sheet and an increase in the cross-tail current are well-described phenomenological aspects of the substorm growth phase in Earth's magnetotail [*Petrukovich et al.*, 2007, and references therein]. During that phase the current sheet thickness decreases dramatically with time, from a few Earth radii to less than 1 R_E (down to the order of hundreds of kilometers); that is, it becomes comparable with the ion thermal gyroradius [*Sergeev et al.*, 1990; *Sanny et al.*, 1994; *Zhou et al.*, 2009].

[4] This plasma sheet thinning leads to demagnetization of a large fraction of neutral sheet ions [*Zhou et al.*, 2009]; electrons, however, are expected to remain magnetized. Intensification of the relative drift between ions and electrons may result in ion tearing [*Schindler*, 1974; *Sitnov et al.*, 2002] of the current sheet and/or cross-field current instability, leading to current disruption [*Lui*, 1996]. Therefore, a study of current carriers within such thin current sheets is important for understanding the dynamics of the plasma sheet related to different substorm phases.

[5] Under stationary conditions, the drift velocity of the s component fluid in anisotropic plasmas, as derived from the momentum equation, is

$$\boldsymbol{v}_s = \frac{\mathbf{E}\times\mathbf{B}}{B^2} + \frac{1}{q_s n_s B^2}\boldsymbol{B}\times\nabla P_{s\perp} + \frac{1}{q_s n_s B^2}\boldsymbol{B}\times\nabla \cdot\left[\left(P_{s//}-P_{s\perp}\right)\frac{\boldsymbol{BB}}{B^2}\right]. \quad (1)$$

The current density, $\boldsymbol{J}_\perp$, perpendicular to the magnetic field, $\boldsymbol{B}$, in a collisionless plasma therefore includes two terms: one containing the pressure gradient perpendicular to $\boldsymbol{B}$, and the other, the pressure anisotropy term $(P_{//}-P_\perp)$ divided by the radius of curvature of the local magnetic field [e.g., *Mitchell et al.*, 1990], i.e.,

$$\boldsymbol{J}_\perp = \frac{\boldsymbol{B}}{B^2}\times\left[\nabla P_\perp - \left(\frac{P_{//}-P_\perp}{R_c}\right)\boldsymbol{n}\right], \quad (2)$$

where $P_{//}$ ($P_\perp$) is the plasma pressure along (across) $\boldsymbol{B}$, R_c the local radius of curvature of $\boldsymbol{B}$, and $\boldsymbol{n}$ the unit normal vector outward from the center of curvature. Thus, the excess electron pressure parallel to $\boldsymbol{B}$ will contribute to $\boldsymbol{J}_\perp$ in a stretched field reversal region.

[6] *Mitchell et al.* [1990] showed that during the early growth phase of a substorm, thermal electrons (~1 keV, adiabatic) can contribute significantly to the cross-tail current, due to pressure anisotropy (excess parallel pressure relative to perpendicular pressure). In the late growth phase, however, nonadiabatic ion motion is sufficient to support the entire current.

[7] A number of studies have shown that flows in the near-Earth and midtail plasma sheet tend to occur in 10 min time scale flow enhancements (bursty bulk flow events) that contain embedded velocity peaks ~1 min in duration (flow bursts). An earthward pressure gradient that is anticipated ahead of the significant earthward transport of the northward magnetic flux [*Angelopoulos et al.*, 1994] causes the flow bursts to pile up at the inner edge of the plasma sheet. The resulting enhancement in magnetic pressure may cause the stopping point of the flow bursts to move tailward [*Shiokawa et al.*, 1997]. Indeed, *Baumjohann et al.* [1999] reported an observation of dipolarization at 10–15 R_E expanding tailward at an average velocity of 35 km/s; while more recently, *Panov et al.* [2010a, 2010b] reported on THEMIS observations that demonstrate the actual stopping of the flow caused by the intense pressure gradients. The pressure gradients build up once the individual flow bursts reach the inner magnetosphere, causing the incoming plasma to recoil and oscillate in the 1–2 min period range multiple times.

[8] Large-scale magnetic field dipolarization during a substorm is thought to be due to reduction of the total cross-tail current in the near-Earth region and related to the buildup of the substorm current wedge [*McPherron*, 1979]. According to *McPherron et al.* [1973], the current wedge is responsible for the diversion of part of the cross-tail current into the auroral ionosphere. Initial current wedge formation has been referred to as the current disruption (CD) process [*Lui et al.*, 1988]. Current disruption starts in a small equatorial area (~1 R_E^2) [*Ohtani et al.*, 1991] and propagates longitudinally [*Nagai*, 1982] and tailward at ~200 km/s during the course of a substorm [*Jacquey et al.*, 1991; *Ohtani et al.*, 1992a, 1992b]. The current wedge may be present over a large region of the nightside magnetosphere, extending as far downtail as 30 R_E [*Ohtani et al.*, 1992a].

[9] A dipolarization front, observed within a bursty bulk flow (BBF), is a thin boundary layer separating hot, tenuous BBF plasma from the ambient plasma sheet [*Nakamura et al.*, 2002; *Runov et al.*, 2009, 2010]. It represents another class of thin current sheets in the magnetotail: a vertical current sheet, strongly localized approximately along the X direction [*Sergeev et al.*, 2009]. The thickness of such structures can be as small as the ion inertial length [*Runov et al.*, 2009]. This scale suggests decoupled motion of ions and electrons. An important question therefore is whether the vertical current is due to electron pressure gradients/anisotropy or ion pressure gradients/anisotropy. Another important question is how the dipolarization fronts interact with the preexisting cross-tail current and the inner magnetosphere to contribute to the global substorm current wedge. If the current wedge extends to 30 R_E, as noted in the *Ohtani et al.* [1992a] study, do the reconnection sites retreat downtail [*Angelopoulos et al.*, 1996a], or do the two processes (namely, the earthward side of the reconnection ejecta and the current disruption) merge and become indistinguishable at larger distances?

[10] In this paper, we report results of a case study that examines current carriers ahead of and within dipolarization fronts using THEMIS measurements. Our results suggest that the dominant cross-tail current contributors during the growth phase are ions rather than electrons from pressure anisotropy, as was inferred from earlier studies. We also investigated the relative contribution from ions and electrons within the dipolarization front and conclude that the electrical current arising from the electron pressure gradient is a dominant contributor to the current density under such

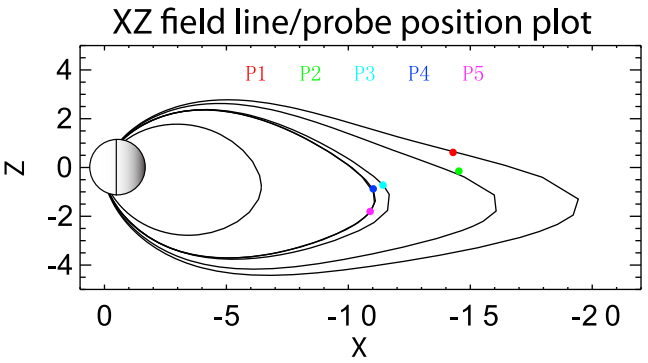

Satellite	Color	X	Y	Z	Neutral Sheet
THEMIS-A (P5)		-10.909	2.812	-1.812	-0.8
THEMIS-B (P1)		-14.234	2.77	0.601	1.7
THEMIS-C (P2)		-14.49	2.625	-0.161	0.9
THEMIS-D (P3)		-11.42	1.771	-0.726	0.4
THEMIS-E (P4)		-11.032	2.686	-0.884	0.2

Figure 1. Projections of THEMIS probes in X-Z_{GSM} and X-Y_{GSM} plane and neutral sheet location at ~0600 UT on 23 March 2009.

conditions. Finally, we report on the tailward evolution of the substorm current wedge in the context of the earthward flows using the fortuitous presence of two probe groups at two different downtail distances near the same meridian.

2. Observations

[11] We examined THEMIS observations during a substorm, when the probes were in major conjunction, i.e., tail aligned, with a Y separation of less than 2 R_E. Data from the THEMIS Fluxgate Magnetometer (FGM) [*Auster et al.*, 2008], Electric Field Instrument (EFI) [*Bonnell et al.*, 2008], Electrostatic Analyzer (ESA) [*McFadden et al.*, 2008], and Solid State Telescope (SST) [*Angelopoulos*, 2008] were used in this study.

[12] During this major conjunction on 23 March 2009, two pairs of mostly Z-separated THEMIS probes, P4/P5 and P1/P2, were located at $X = -11$ R_E and -14.5 R_E, respectively (Figure 1). P3 was separated from the inner pair (P4/P5) by ~0.5 R_E and ~1 R_E in the X and Y directions, respectively. The inner pair was able to observe the neutral sheet vicinity, while the outer pair (P1/P2) was located slightly farther away, near the outer plasma sheet. Note that in this paper we refer to X, Y, Z as the three orthogonal directions in the geocentric solar magnetospheric (GSM) coordinate system.

[13] Figure 2 shows an overview of THEMIS measurements between 0400 UT and 0700 UT. The THEMIS pseudo-*AE* index [*Russell et al.*, 2008] is provided in Figure 2a; the time series of X and Z magnetic field components at P5/P4 (located at the same X and Y and separated by ~1 R_E in Z) and P3 (separated from P5/P4 by ~0.5 R_E and ~1 R_E in the X and Y directions) are shown in Figures 2c, 2d, and 2b; the three components of the electric field data (in GSM coordinates with offsets removed) observed by P4 are plotted in Figures 2e and 2f (in order to show the magnitude of the electric field variations, we enlarged the data in Figure 2f); the following panels depict electron (Figure 2g) and ion (Figure 2h) energy spectra, ion density (Figure 2i), plasma and magnetic pressures (Figure 2j). Figure 2k shows the current density from ion bulk flow in the probe frame of reference $J_{iy} = (nev_i)_y$ (black), electron $\mathbf{E} \times \mathbf{B}$ drift $J_{\mathbf{E}\times\mathbf{B}} = -(ne\boldsymbol{v}_{\mathbf{E}\times\mathbf{B}})_y$ (blue), and electron pressure gradient $J_{ey\_dia} = -\frac{B_x \times \partial P_{e\perp}/\partial z}{B^2}$ (green). Figure 2l compares the local current density estimated from Harris model (black) with the current density calculated from plasma moments (red).

[14] During the first 2 h, the geomagnetic environment was quiet. The THEMIS pseudo-*AE* index (2a, consistent with the Kyoto geomagnetic *AE* index) began to increase gradually at 0450 UT, followed by a sudden rise from about 30 nT to about 200 nT within 10 min starting at 0605 UT. The IMF B_z remained southward during the event. IMF B_y was negative. The solar wind dynamic pressure was steady at about 0.6–0.8 nPa, and the velocity of the solar wind V_x was nominal (410 km/s). Other activity indices were also very small (*Dst* ~ −10 nT, *Kp* ~ 0+).

[15] To ensure accurate flow velocities, we removed sources of contamination, such as photoelectrons in the electron detector [*McFadden et al.*, 2008] and background high-energy electrons in the ion detector when necessary. We included the energetic particle instrument (SST) contribution to the ion moments, after removing sunlight and electronic contamination.

[16] As shown in Figures 2b–2d, during the low *AE* interval (0400–0603 UT), P5 (P3), located in the southern (northern) half of the plasma sheet, detected a gradual increase in $|B_x|$ accompanied by a decrease in B_z. At the same time, P4, located near the neutral sheet ($B_x < 5$ nT), observed small fluctuations in B_x and a pronounced decrease in B_z. These signatures suggest thinning and stretching of the current sheet [*Petrukovich et al.*, 2007]. The Z separation of P4 and P5 enables estimation of the current density at location of P4 (black line in Figure 2l) by fitting magnetic field data from these two probes into a Harris sheet model [*Harris*, 1962]. Between 0430 and 0600 UT the current density increased by a factor of 3, from 2 to 6 nA/m^2, indicating current sheet thinning during the growth phase of the substorm.

[17] The inconsistency between the ion-contributed current density (black curve in Figure 2k) and the current density from the Harris model (black curve in Figure 2l) at P4 indicates that the current cannot be supported by ions alone, and that the assumption of electron stationarity is incorrect. As illustrated in Figure 2k, the diamagnetic current from the electron pressure gradient (green line in Figure 2k) may contribute up to 60% to the total current at ~0540 UT. In calculating the local current density from particle con-

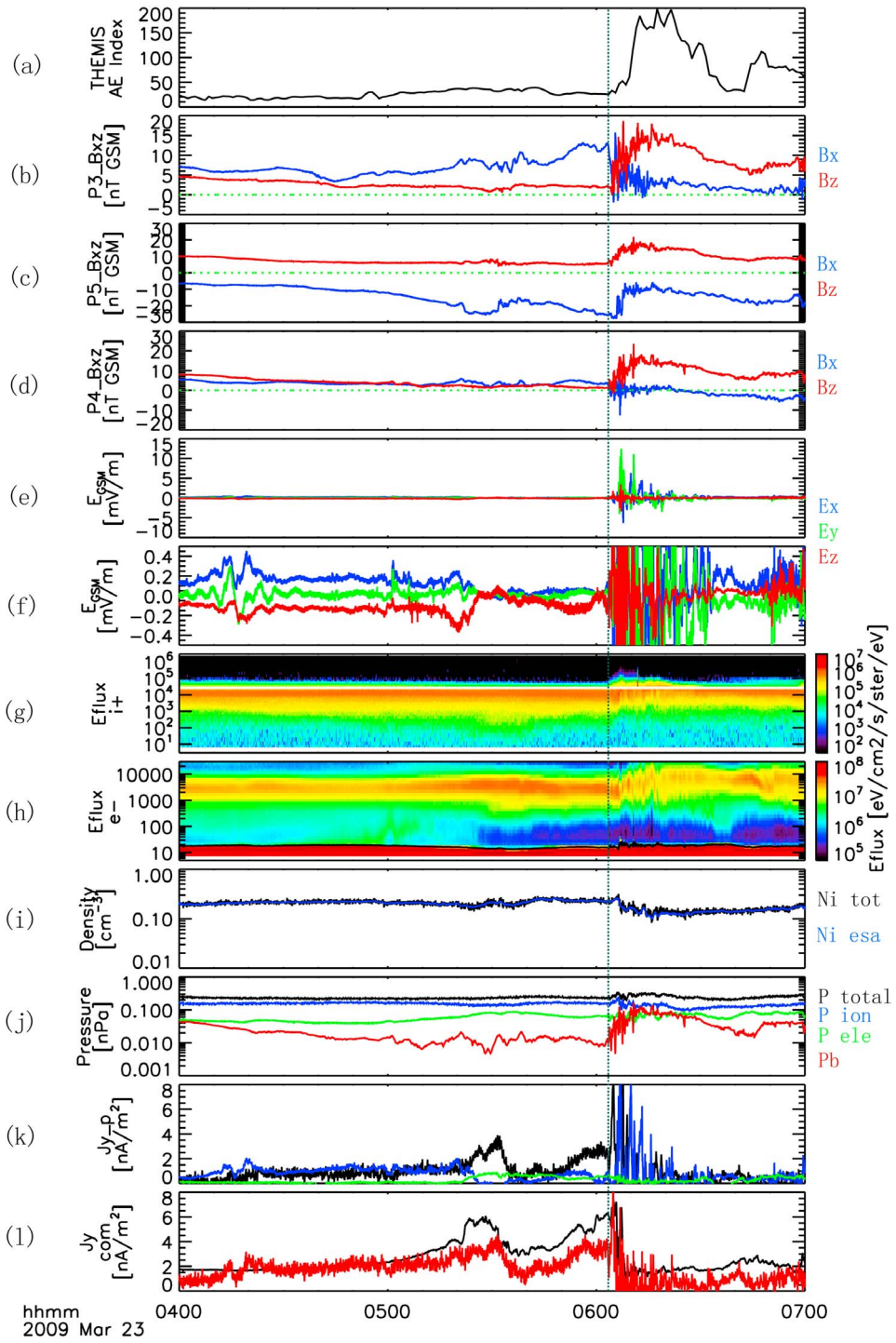

Figure 2. Overview of the event, with a vertical dashed line indicating arrival of dipolarization fronts at P4. From top to bottom: (a) THEMIS pseudo-*AE* index; the *X*, *Z* component of magnetic field data in the geocentric solar magnetospheric (GSM) coordinate system for (b) P3, (c) P5, and (d) P4; (e, f) P4 observation of electric field data (after removing the offsets) in GSM coordinate system; time evolution of the (g) ion and (h) electron energy flux; (i) ion density profile; (j) plasma and magnetic pressure profile; (k) current density from ion bulk flow (black), electron $\mathbf{E} \times \mathbf{B}$ drift (blue), and electron pressure gradient between the two probes (green); and (l) comparison between the local current density from Harris model (black) and that from particle contributors (including ion bulk flow and the electron drift from pressure gradient between the two probes) for P4.

Table 1. Minimum Variance Analysis Results for P4/P3 Observations[a]

SC[b]	Time (UT)	λ_1, λ_2, λ_3	R_1	R_2	R_3
P4	0603:40	3.84, 0.25, 0.09	−0.58, −0.17, 0.79	−0.18, 0.98, 0.08	0.79, 0.09, 0.60
P3	0604:39	3.59, 0.11, 0.01	0.36, 0.55, −0.76	−0.04, −0.80, −0.60	0.93, −0.24, 0.27
P4	0606:23	9.66, 0.86, 0.03	−0.15, −0.67, −0.73	−0.33, −0.66, 0.67	0.93, −0.34, 0.12
P4	0606:50	16.65, 1.39, 0.07	−0.60, −0.46, 0.65	0.23, 0.67, 0.70	0.76, −0.58, 0.30

[a]Time (UT) indicates the instances of the center of positive B_z variations. MVA was performed over a variable window around the specified time. Results with the best ratio of λ_2 and λ_3 are shown.
[b]Name of spacecraft.

tributors in Figure 2l, we utilized the ion bulk velocity from measurements and electron drift retrieved from equation (1), i.e.,

$$J_y = ne(\boldsymbol{v}_i - \boldsymbol{v}_{\mathbf{E}\times\mathbf{B}})_y - \frac{B_x \times {}^{\partial Pe_\perp}/_{\partial z}}{B^2}. \quad (3)$$

The electron pressure gradient was estimated using the pressure difference between the two probes (P4/P5). Current from electron pressure anisotropy was evaluated and found negligibly small by comparison. To obtain $\mathbf{E} \times \mathbf{B}$ drift for particles, we calculated the third component of the electric field (E_{z_DSL}) using the $\boldsymbol{E} \cdot \boldsymbol{B} = 0$ approximation. The offsets of the other two components were removed based on typical offset values in a similar density/temperature environment, $E_{x\_offset} \sim -0.8$ mV/m and $E_{y\_offset} \sim 0$ mV/m, and consistent with average values earlier during this day.

[18] As seen in Figures 2c and 2d, at ~0603 UT, P4 and P5 detected a rapid increase in the Z component of the magnetic field accompanied by a decrease in the X component: a dipolarization front. The electric current density within a dipolarization front can no longer be obtained by taking advantage of the Z separation of P4 and P5. Instead, one may reconstruct the electric current profile by converting the time derivatives of the magnetic field ($\partial B_z/\partial t$) to its space derivatives ($\partial B_z/\partial n$), where n is the normal direction of the dipolarization front. To examine the orientation of the dipolarization front detected by P4 and P3 (separated by ~0.5 R_E in the Y direction) close to the neutral sheet, Minimum Variance Analysis (MVA) [*Sonnerup and Scheible*, 1998] was applied to the magnetic field time series capturing the fronts. The MVA results are summarized in Table 1. The three MVA eigenvectors, $\boldsymbol{R_1}$, $\boldsymbol{R_2}$, and $\boldsymbol{R_3}$, corresponding to the three eigenvalues, λ_1, λ_2, and λ_3, define the maximum, intermediate, and minimum variance directions in the GSM coordinates, respectively. Because $\lambda_2/\lambda_3 > 10$, $\boldsymbol{R_3}$ was interpreted as the front normal vector. The normals are close to the X_{GSM} direction. The evolution of the Z_{GSM} component basically matches the maximum variance component of the magnetic field data for the first two fronts; but there is an offset between these two methods for the third front. Using the $\mathbf{E} \times \mathbf{B}$ drift velocity in the minimum variance direction (i.e., the front normal direction), we converted time differences $\partial B_z/\partial t$ to distances ($\partial B_z/\partial t \cdot v_n$) and reconstructed the profile of $\partial B_z/\partial n$, i.e., electric current density at the front.

[19] To address the question of current carriers, we examined contributions to the current from electrons and ions within dipolarization fronts. To do this, we investigated electron pressure profiles at each front. Figure 3 shows a comparison of the electron, magnetic pressures, and P_{sum} (sum of electron and magnetic pressures) and the current density from B_z change (green) and electron pressure gradient (black) for three fronts observed by P4. The current density from ion polarization drift is also included for the third front (blue curve in third panel of Figure 3c represents the current density from electron pressure gradient plus ion polarization drift). The typical duration of one dipolarization is on the order of 1–10 s, so we could not use the nominal observations for particle moments from the ESA/THEMIS instrument (with a 3 s cadence) to resolve the structure. Since the electrons are fast and most probably gyrotropic, we used the electron flux measured in the perpendicular sectors with the particle detector rotating 16 times per spin to give much higher temporal resolution data (with a 3/16 s cadence) (similar to Figure 3 of *Sergeev et al.* [2009]). Error bars associated with this calculation of electron perpendicular pressure are overlain in the data (second panel in Figure 3), once every fifth data point. Since ions are not necessarily gyrotropic, we could not apply this technique to get higher temporal resolution data for ion moments. So we first estimated the current contribution from the electron pressure gradient within the dipolarization fronts, $J_y \sim \frac{B_z \times {}^{\partial Pe_\perp}/_{\partial n}}{B^2}$.

[20] A clear anticorrelation between the magnetic pressure (green) increasing at the fronts and the electron perpendicular pressure (black) decreasing at the fronts is visible (second panel). Moreover, the current density estimated from the change in B_z and the diamagnetic current due to the perpendicular electron pressure gradient ($J_y \sim \frac{B_z \times {}^{\partial Pe_\perp}/_{\partial n}}{B^2}$) are of the same order of magnitude (third panel).

[21] To complete our investigation of current carriers within the vertical current sheet, we also checked the ion diamagnetic current $J_{iy\_dia} = ne(\boldsymbol{v}_i - \boldsymbol{v}_{\mathbf{E}\times\mathbf{B}})_y$ within dipolarization fronts using nominal measurements for ion moments (with a 3 s cadence). It is ~0.5–5 nA/m^2, almost an order of magnitude smaller than the current from the electron pressure gradient. This indicates that the vertical current sheet density is mainly supported by the net electron current resulting from the perpendicular pressure gradient. The current density associated with the thin dipolar structure is ~30 nA/m^2, which is 10 times larger than the horizontal cross-tail current density.

[22] For the front at around 0606:50 UT (3c), the increase in P_{sum} (second panel in Figure 3c) is pronounced. P_{sum} should be almost constant if the vertical current is primarily supported by the electron pressure gradient. To explain this discrepancy, we estimated the polarization current

$$J_{y\_polar} = nq \frac{{}^{\partial E_y}/_{\partial t}}{\Omega_c B}, \quad (4)$$

where Ω_c is the ion gyration frequency. Since the polarization current density is inversely proportional to the cyclotron frequency, the main contribution to it is from ions (electrons

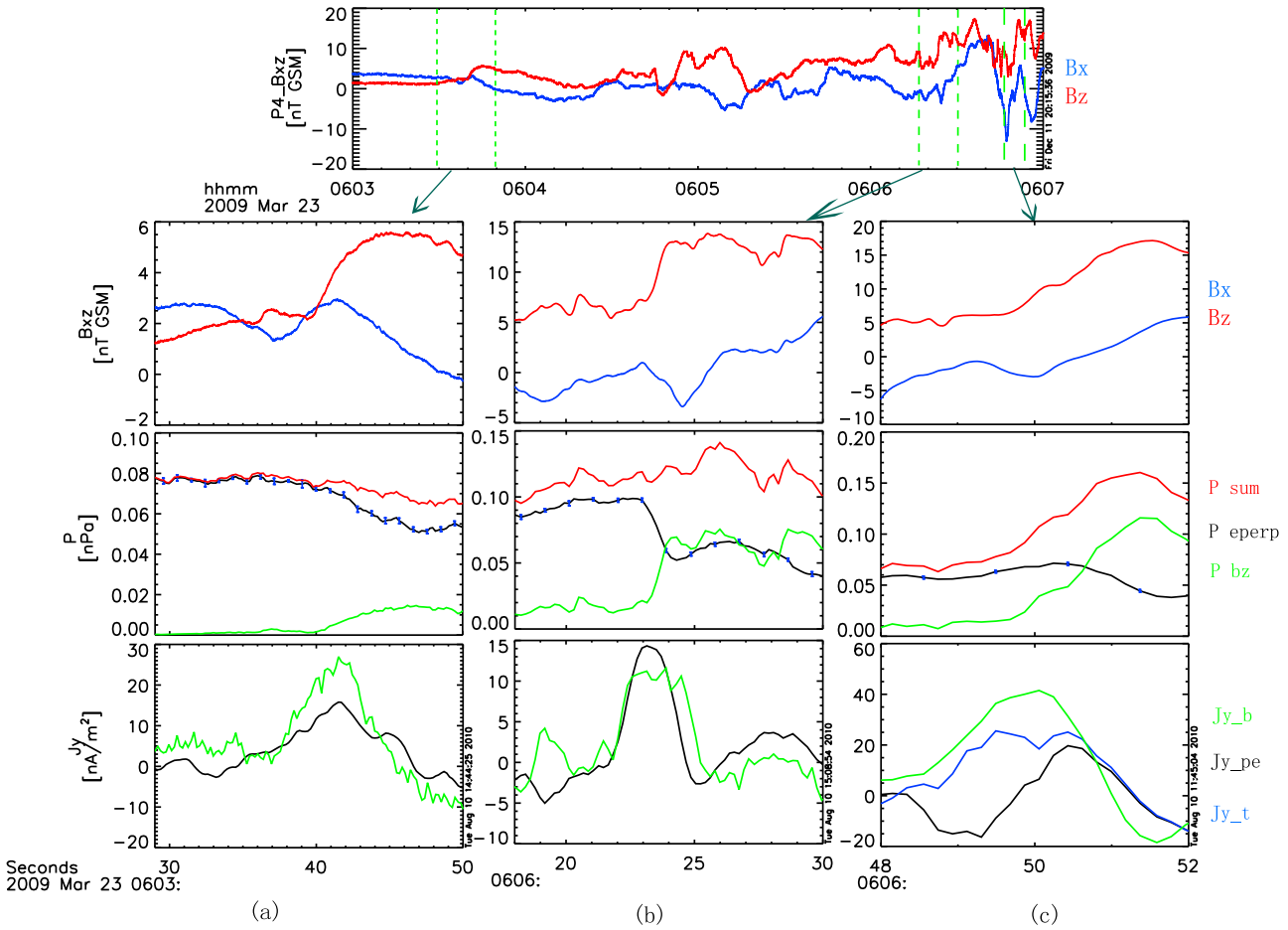

Figure 3. Pressure and current density for three dipolarization fronts observed by P4: magnetic field (X_{GSM}, Z_{GSM} component); perpendicular electron plasma pressure (black), magnetic pressure $\frac{B_z^2}{2\mu_0}$ (green), and the sum of these two pressures (red); and current density from B_z change (green) and electron pressure gradient (black, plus the polarization current in blue) within the dipolarization front.

gyrate too fast to experience a polarization drift). By using (4) we find that the polarization current is mostly evident from 0606:48–0606:50, which almost fills in the gap between the current density from the B_z change and that from the electron pressure gradient (third panel in Figure 3c).

3. Summary and Discussion

[23] Using multipoint observations from three horizontally and vertically separated THEMIS probes in the premidnight plasma sheet at $X = -11$ R_E, near the onset time of an isolated substorm, we estimated current densities in the cross-tail current sheet and the thin current sheet associated with approaching dipolarization fronts. By comparing current densities estimated from magnetic field measurements with those derived from ion and electron distribution function moments, we identified the particles that are the main contributors to the current at the growth phase and at the dipolarization front.

[24] The cross-tail current density evolution during the growth phase increased by a factor of 3 (2–6 nA/m^2) as measured over a 1 R_E vertical inner probe separation, indicating sheet thinning. Earlier studies, using Cluster data, showed an increase in cross-tail current density from ~2 to ~8 nA/m^2 during the growth phase [*Petrukovich et al.*, 2007], which is in agreement with our results. By investigating plasma sheet flapping events at distances from 12 to 18 R_E, *Sergeev et al.* [1998] reported an estimation of the cross-tail current density of 10–30 nA/m^2 around substorm onset. The result from *Sergeev et al.* [1990] (lobe field of ~40 nT, current sheet thickness of ~0.2 R_E at distance of ~9 R_E) also indicated a peak cross-tail current density of ~25 nA/m^2 at the neutral sheet near the end of the substorm growth phase, by interpreting the magnetic field variation as a Harris sheet model. Both of these studies are in agreement with our results.

[25] The good agreement between the current density estimated from magnetic field measurements and the one derived from particle and electric field measurements (Figure 2l) allows us to conclude that prior to the dipolarization front, both electrons and ions contributed to the cross tail current (horizontal), with the dominant contribution coming from ions. The electron pressure gradient may occasionally account for up to 60% of the total current density. We conclude that this event differs from that of *Mitchell et al.* [1990], who showed that ions did not take over from thermal

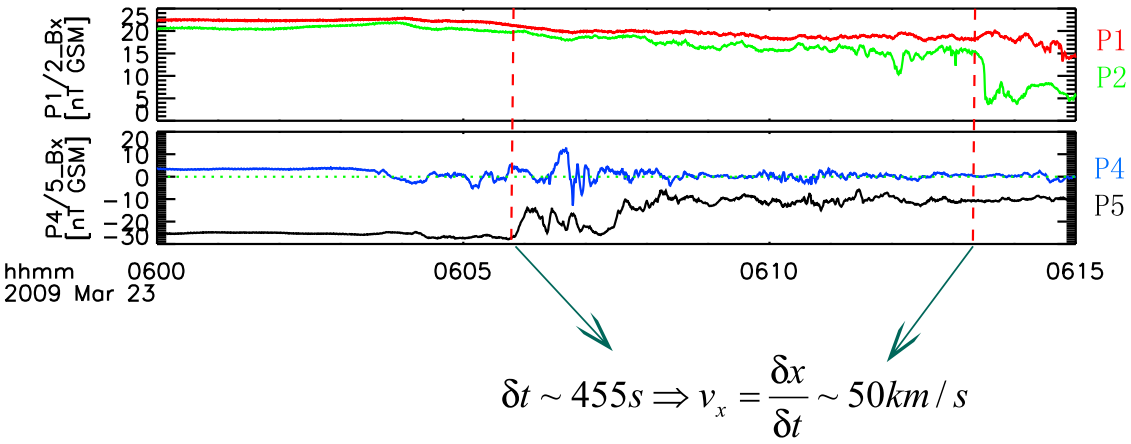

Figure 4. B_x evolution for the two pairs of probes (P1/P2 and P4/P5), from which we can infer the propagation velocity of the dipolarization front along the magnetotail.

electrons as dominant current contributors until the late growth phase.

[26] Observations of magnetic field and plasma moments at the dipolarization front correspond to characteristic BBF signatures [*Angelopoulos et al.*, 1994]: increase in bulk velocity and magnetic pressure and decrease in plasma density and pressure. The MVA normal directions suggest dawnward deflection of the dipolarization region, which is consistent with earlier observations [*Nakamura et al.*, 2002; *Runov et al.*, 2009]. Figure 4 shows the magnetic field observations of the two pairs of probes (P4/P5, P1/P2). Between 0605 and 0615 UT, similar front-like variations in B_x were detected consecutively by the P4/P5 and P1/P2 probes. From these variations, we can determine the propagation direction of the vertical front and estimate its propagation velocity, as shown in Figure 4. In this event, the dipolarization front expanded tailward at a velocity ~50 km/s, accompanied by earthward flow carrying piled-up fluxes inward. This result is also consistent with the estimation from variations in B_z detected by P4 and P3 successively, which imply a tailward velocity of ~40 km/s.

[27] The fact from our observations that the current wedge retreats tailward from ~11 R_E to ~15 R_E at a velocity ~50 km/s, is consistent with the reported velocity of tailward retreat of the plasma sheet recovery [*Baumjohann et al.*, 1999], though a factor of two smaller than previous current disruption observations [*Jacquey et al.*, 1991; *Ohtani et al.*, 1992a, 1992b]. It is possible that the slow retreat relative to other current disruption observations is due to the weak nature of the substorm under study.

[28] With the arrival of the dipolarization front from the tail, the current density in the horizontal cross-tail current sheet (2–6 nA/m^2) decreases. As a thin boundary, the dipolarization front may be considered a quasi-1D vertical current sheet carrying significant current density. In our case, the current density in the vertical current sheet due to the thin dipolar structure was ~30 nA/m^2. Our analysis shows that the dipolarization front (a jump in B_z) in this event was supported mainly by the diamagnetic current due to the strong pressure gradient at the front. On occasion, the polarization current (on the order of 20 nA/m^2) can be as significant as the electron pressure gradient current, even though they may occur at different times.

[29] Nonetheless, there is still some discrepancy between the current density estimated from the B_z jump and that derived from particle and electric field data. The source of errors may lie in the calculation of particle moments from distribution functions. Despite the lack of quantitative precision, the presented case study demonstrates qualitative agreement between current density estimates obtained from the magnetic field and particle measurements, which provides valuable, new information on the physics of dipolarization fronts. Although in our event the vertical current sheet was mainly supported by electron diamagnetic current due to pressure gradient, this may not be the case for other events. Further study is needed to address the generality of our conclusions.

[30] In closing, we note the importance of understanding the interaction between incoming dipolarization fronts and the preexisting, thin, horizontal current sheet. The arrival of the fronts disturbs the cross-tail current distribution, but in fact enhances the local cross-tail current density. The intensity of the current at the front (~50 nA/m^2) is ~10 times larger than the horizontal cross-tail current (~1 nA/m^2), but the scale size ($\delta x \sim 0.1\ R_E$, $\delta z \sim 1\ R_E$) is ~10 times smaller than the cross-tail current ($\delta x \sim 10\ R_E$, $\delta z \sim 0.5\ R_E$). Therefore the total vertical current (~2×10^5 A) is comparable to (consistent with) the total cross-tail current (~2×10^5 A). The intense cross-tail current is present at the front to support the boundaries of the reconfigured magnetic field. As the dipolarized magnetic flux bundle arrives, it perturbs both the local and the global current systems. The local current system of these plasma-depleted flux tubes, termed "bubbles" has been discussed by *Pontius and Wolf* [1990] and *Nakamura et al.* [2001] and reviewed by *Wolf et al.* [2006]. It entails a redirection of the cross-tail current sheet into the ionosphere at the dawn side and out of the ionosphere at the dusk side. However, the observed flow bursts therein often result in a permanent (i.e., prolonged, lasting tens of minutes) dipolarization of the plasma sheet in the local time sector of the observations and a significant reduction in the tail lobe flux. Thus, while the dipolarization

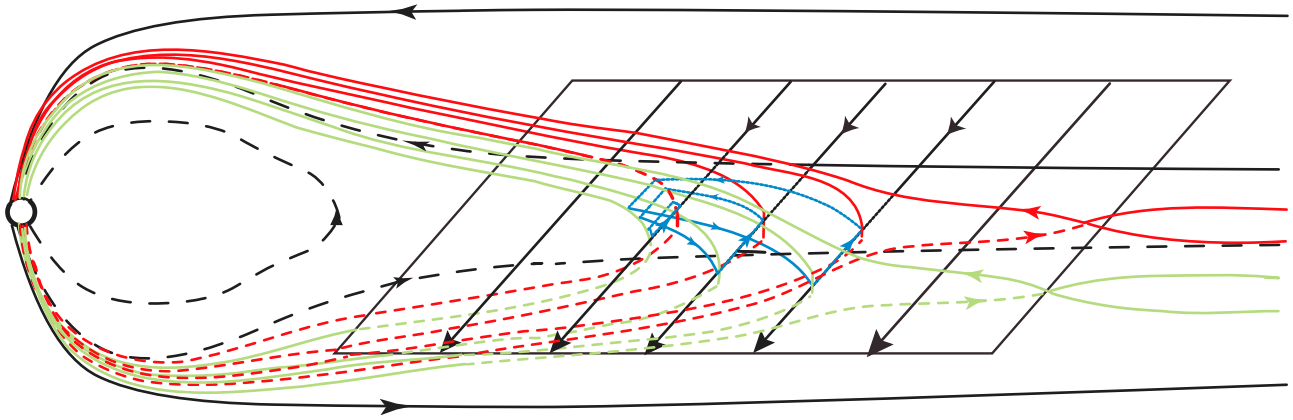

Figure 5. Cross-tail current diversion at the meridian of the depolarized flow burst. With the arrival of the flow burst, originally stretched tail-like field lines become more dipolarized (red at the dawn side of the front and green at the dusk side of the front). Outside the meridian of the dipolarized flow burst, the field lines remain stretched (black field lines), and the current sheet retains its horizontal structure (black lines along neutral sheet). Redistribution of the horizontal cross-tail current at the sector of the dipolarized flow burst occurs in the radial direction (earthward/tailward) via cross-field currents (blue lines) and feeding the intense duskward current of the dipolarization front (blue azimuthal lines).

front is sharp (500 km) and kinetic in nature, the effects of flux bundle arrival are permanent over the local time sector, as proposed by *Angelopoulos et al.* [1996b] (see their Figure 17). As the tail lobe flux is expected to be reduced by the incoming front, due to the tail reconnection that generated it, so is the total cross-tail current tailward of the dipolarization front. However, a more dramatic effect is the reduction in the cross-tail current across the local time sector of the dipolarization front, because the permanent dipolarization behind the front results in local relaxation of the cross-tail current. At the same time, typical plasma sheet behavior on either side of the dipolarization front is to retain its structure, at least initially. Thus the typical, presubstorm horizontal current is expected to flow along the plasma sheet at local times away from the dipolarization fronts, because tail spacecraft do not observe dipolarization fronts or total pressure changes unless they are within the fast flow channels. The magnetic topology at the dawn and dusk edges of the flow burst (strong B_z inside and low B_z outside) necessitates cross-field currents in the earthward and tailward directions respectively. These are not necessarily field aligned. Also, the fact that the front is not evident in the magnetic field data ahead of its arrival at a satellite suggests that the field aligned currents do not initially extend all the way to the ionosphere. The above discussion suggests that the horizontal cross-tail current is interrupted abruptly on the side of the front and within the front, but not ahead of it or on its sides. Thus, not only the side boundary layer current, but also the cross-tail current must close through/around the flux bundle but not through the ionosphere. It is therefore reasonable to expect that these currents will close through the dipolarization front current. The situation is explained pictorially in Figure 5.

[31] When the dipolarization front approaches Earth, it encounters the strong field of the near-Earth region, at which point there is no demand for duskward current at the dipolarization front (the "front" has reached the inner edge of the tail current and vanishes, as the flow burst flux merges with the flux of the inner magnetosphere). The earthward/tailward current densities at the sides of the flow burst must therefore close into the ionosphere, with field-aligned currents along the dawn and dusk edges of the dipolarized flux bundle. This is the substorm current wedge in its elemental form. In this view, dipolarization fronts are a transient current layer carrying cross-tail current that has been diverted across the local time sector of the flow burst, until ionospheric connection takes place upon arrival of the front at Earth.

[32] **Acknowledgments.** We thank P. L. Pritchett, M. Sitnov, and M. Fujimoto for useful discussions and B. Kerr and P. Cruce for their assistance with the software. We also thank J. Hohl for her help with editing. We acknowledge NASA contracts NAS5–02099 and NNX08AD85G, the German Ministry for Economy and Technology, and the German Center for Aviation and Space (DLR), contract 50 OC 0302. *AE*, *Kp*, and *Dst* data were provided by the World Data Center for Geomagnetism in Kyoto. The OMNI data are available on CDAWeb. We are thankful for the use of NASA/SPDF's SSCWeb 4-D Orbit Viewer software for satellite location information.

[33] Robert Lysak thanks the reviewers for their assistance in evaluating this paper.

References

Angelopoulos, V. (2008), The THEMIS mission, *Space Sci. Rev.*, *141*, 5–34, doi:10.1007/s11214-008-9336-1.

Angelopoulos, V., C. Kennel, F. Coroniti, R. Pellat, M. Kivelson, R. Walker, C. Russell, W. Baumjohann, W. Feldman, and J. Gosling (1994), Statistical characteristics of bursty bulk flow events, *J. Geophys. Res.*, *99*(A11), 21,257–21,280, doi:10.1029/94JA01263.

Angelopoulos, V., et al. (1996a), Tailward progression of magnetotail acceleration centers: Relationship to substorm current wedge, *J. Geophys. Res.*, *101*(A11), 24,599–24,619, doi:10.1029/96JA01665.

Angelopoulos, V., et al. (1996b), Multipoint analysis of a bursty bulk flow event on April 11, 1985, *J. Geophys. Res.*, *101*(A3), 4967–4989, doi:10.1029/95JA02722.

Angelopoulos, V., et al. (2008), First results from the THEMIS mission, *Space Sci. Rev.*, *141*, doi:10.1007/s11214-008-9378-4.

Auster, H. U., et al. (2008), The THEMIS fluxgate magnetometer, *Space Sci. Rev.*, *141*, 235–264, doi:10.1007/s11214-008-9365-9.

Baumjohann, W., M. Hesse, S. Kokubun, T. Mukai, T. Nagai, and A. A. Petrukovich (1999), Substorm dipolarization and recovery, *J. Geophys. Res.*, *104*(A11), 24,995–25,000, doi:10.1029/1999JA900282.

Baumjohann, W., et al. (2007), Dynamics of thin current sheets: Cluster observations, *Ann. Geophys.*, *25*, 1365–1389, doi:10.5194/angeo-25-1365-2007.

Bonnell, J. W., et al. (2008), The electric field instrument (EFI) for THEMIS, *Space Sci. Rev.*, *141*, 303–341, doi:10.1007/s11214-008-9469-2.

Harris, E. G. (1962), On a plasma sheath separating regions of oppositely directed magnetic field, *Nuovo Cimento*, *23*, 115–121, doi:10.1007/BF02733547.

Jacquey, C., J. A. Sauvaud, and J. Dandouras (1991), Location and propagation of the magnetotail current disruption during substorm expansion: Analysis and simulation of an ISEE multi-onset event, *Geophys. Res. Lett.*, *18*(3), 389–392, doi:10.1029/90GL02789.

Lui, A. T. Y. (1996), Current disruption in the Earth's magnetosphere: Observations and models, *J. Geophys. Res.*, *101*(A6), 13,067–13,088, doi:10.1029/96JA00079.

Lui, A. T. Y., R. E. Lopez, S. M. Krimigis, R. W. McEntire, L. J. Zanetti, and T. A. Potemra (1988), A case study of magnetotail current sheet disruption and diversion, *Geophys. Res. Lett.*, *15*(7), 721–724, doi:10.1029/GL015i007p00721.

McFadden, J. P., et al. (2008), The THEMIS ESA plasma instrument and in-flight calibration, *Space Sci. Rev.*, *141*, 277–302, doi:10.1007/s11214-008-9440-2.

McPherron, R. L. (1979), Magnetospheric substorms, *Rev. Geophys. Space Phys.*, *17*, 657–681, doi:10.1029/RG017i004p00657.

McPherron, R. L., C. T. Russell, and M. P. Aubry (1973), 9. Phenomenological model for substorms, *J. Geophys. Res.*, *78*(16), 3131–3149, doi:10.1029/JA078i016p03131.

Mitchell, D. G., D. J. Williams, C. Y. Huang, L. A. Frank, and C. T. Russell (1990), Current carriers in the near-Earth cross-tail current sheet during substorm growth phase, *Geophys. Res. Lett.*, *17*(5), 583–586, doi:10.1029/GL017i005p00583.

Nagai, T. (1982), Observed magnetic substorm signatures at synchronous altitude, *J. Geophys. Res.*, *87*(A6), 4405–4417, doi:10.1029/JA087iA06p04405.

Nakamura, R., W. Baumjohann, R. Schödel, M. Brittnacher, V. Sergeev, M. Kubyshkina, T. Mukai, and K. Liou (2001), Earthward flow bursts, auroral streamers, and small expansions, *J. Geophys. Res.*, *106*(A6), 10,791–10,802, doi:10.1029/2000JA000306.

Nakamura, R., et al. (2002), Motion of the dipolarization front during a flow burst event observed by Cluster, *Geophys. Res. Lett.*, *29*(20), 1942, doi:10.1029/2002GL015763.

Ohtani, S., K. Takahashi, L. J. Zanetti, T. A. Potemra, R. W. McEntire, and T. Iijima (1991), Tail current disruption in the geosynchronous region, in *Magnetospheric Substorms*, *Geophys. Monogr. Ser.*, vol. 64, pp. 131–137, AGU, Washington, D. C.

Ohtani, S., S. Kokubun, and C. T. Russell (1992a), Radial expansion of the tail current disruption during substorms: A new approach to the substorm onset region, *J. Geophys. Res.*, *97*(A3), 3129–3136, doi:10.1029/91JA02470.

Ohtani, S., K. Takahashi, L. J. Zanetti, T. A. Potemra, R. W. McEntire, and T. Iijima (1992b), Initial signatures of magnetic field and energetic particle fluxes at tail reconfiguration: Explosive growth phase, *J. Geophys. Res.*, *97*(A12), 19,311–19,324, doi:10.1029/92JA01832.

Panov, E. V., et al. (2010a), Plasma sheet thickness during a bursty bulk flow reversal, *J. Geophys. Res.*, *115*, A05213, doi:10.1029/2009JA014743.

Panov, E. V., et al. (2010b), Multiple overshoot and rebound of a bursty bulk flow, *Geophys. Res. Lett.*, *37*, L08103, doi:10.1029/2009GL041971.

Petrukovich, A. A., W. Baumjohann, R. Nakamura, A. Runov, A. Balogh, and H. Rème (2007), Thinning and stretching of the plasma sheet, *J. Geophys. Res.*, *112*, A10213, doi:10.1029/2007JA012349.

Pontius, D. H., Jr., and R. A. Wolf (1990), Transient flux tubes in the terrestrial magnetosphere, *Geophys. Res. Lett.*, *17*(1), 49–52, doi:10.1029/GL017i001p00049.

Pulkkinen, T., D. Baker, D. Mitchell, R. McPherron, C. Huang, and L. Frank (1994), Thin current sheets in the magnetotail during substorms: CDAW 6 revisited, *J. Geophys. Res.*, *99*(A4), 5793–5803, doi:10.1029/93JA03234.

Runov, A., R. Nakamura, W. Baumjohann, T. L. Zhang, M. Volwerk, H.-U. Eichelberger, and A. Balogh (2003), Cluster observation of a bifurcated current sheet, *Geophys. Res. Lett.*, *30*(2), 1036, doi:10.1029/2002GL016136.

Runov, A., et al. (2006), Local structure of the magnetotail current sheet: 2001 Cluster observations, *Ann. Geophys.*, *24*, 247–262, doi:10.5194/angeo-24-247-2006.

Runov, A., V. Angelopoulos, M. I. Sitnov, V. A. Sergeev, J. Bonnell, J. P. McFadden, D. Larson, K.-H. Glassmeier, and U. Auster (2009), THEMIS observations of an earthward propagating dipolarization front, *Geophys. Res. Lett.*, *36*, L14106, doi:10.1029/2009GL038980.

Runov, A., et al. (2010), Dipolarization fronts in the magnetotail plasma sheet, *Planet. Space Sci.*, doi:10.1016/j.pss.2010.06.006, in press.

Russell, C. T., et al. (2008), THEMIS ground-based magnetometers, *Space Sci. Rev.*, *141*, 389–412, doi:10.1007/s11214-008-9337-0.

Sanny, J., R. L. McPherron, C. T. Russell, D. N. Baker, T. I. Pulkkinen, and A. Nishida (1994), Growth-phase thinning of the near-Earth current sheet during the CDAW 6 substorm, *J. Geophys. Res.*, *99*(A4), 5805–5816, doi:10.1029/93JA03235.

Schindler, K. (1974), A theory of the substorm mechanism, *J. Geophys. Res.*, *79*(19), 2803–2810, doi:10.1029/JA079i019p02803.

Sergeev, V. A., P. Tanskanen, K. Mursula, A. Korth, and R. C. Elphic (1990), Current sheet thickness in the near-Earth plasma sheet during substorm growth phase, *J. Geophys. Res.*, *95*(A4), 3819–3828, doi:10.1029/JA095iA04p03819.

Sergeev, V., V. Angelopoulos, C. Carlson, and P. Sutcliffe (1998), Current sheet measurements within a flapping plasma sheet, *J. Geophys. Res.*, *103*(A5), 9177–9187, doi:10.1029/97JA02093.

Sergeev, V., V. Angelopoulos, S. Apatenkov, J. Bonnell, R. Ergun, R. Nakamura, J. McFadden, D. Larson, and A. Runov (2009), Kinetic structure of the sharp injection/dipolarization front in the flow-braking region, *Geophys. Res. Lett.*, *36*, L21105, doi:10.1029/2009GL040658.

Shiokawa, K., W. Baumjohann, and G. Haerendel (1997), Braking of high-speed flows in the near-Earth tail, *Geophys. Res. Lett.*, *24*(10), 1179–1182, doi:10.1029/97GL01062.

Sibeck, D. G., and V. Angelopoulos (2008), THEMIS science objectives and mission phases, *Space Sci. Rev.*, *141*, 35–59, doi:10.1007/s11214-008-9393-5.

Sitnov, M. I., A. S. Sharma, P. N. Guzdar, and P. H. Yoon (2002), Reconnection onset in the tail of Earth's magnetosphere, *J. Geophys. Res.*, *107*(A9), 1256, doi:10.1029/2001JA009148.

Sonnerup, B. U. Ö., and M. Scheible (1998), Minimum and maximum variance analysis, in *Analysis Methods for Multi-Spacecraft Data*, edited by G. Paschmann and P. Daly, pp. 185–220, Eur. Space Agency, Noordwijk, Netherlands.

Thompson, S. M., M. G. Kivelson, K. K. Khurana, R. L. McPherron, J. M. Weygand, A. Balogh, H. Réme, and L. M. Kistler (2005), Dynamic Harris current sheet thickness from Cluster current density and plasma measurements, *J. Geophys. Res.*, *110*, A02212, doi:10.1029/2004JA010714.

Wolf, R. A., R. W. Spiro, S. Sazykin, F. R. Toffoletto, P. Le Sager, and T.-S. Huang (2006), Use of Euler potentials for describing magnetosphere-ionosphere coupling, *J. Geophys. Res.*, *111*, A07315, doi:10.1029/2005JA011558.

Zhou, X.-Z., et al. (2009), Thin current sheet in the substorm late growth phase: Modeling of THEMIS observations, *J. Geophys. Res.*, *114*, A03223, doi:10.1029/2008JA013777.

V. Angelopoulos, A. Runov, X.-J. Zhang, and X.-Z. Zhou, Institute of Geophysics and Planetary Physics, University of California, Los Angeles, CA 90095, USA. (xjzhang@ucla.edu)

U. Auster, Institut für Geophysik und Extraterrestrische Physik, Technische Universität Braunschweig, Braunschweig D-38106, Germany.

J. Bonnell, D. Larson, and J. P. McFadden, Space Sciences Laboratory, University of California, Berkeley, CA 94720, USA.